

Anti-Agglomerants Affect Gas Hydrate Growth

*Tai Bui¹, Francois Sicard¹, Deepak Monteiro², Qiang Lan², Mark Ceglio², Charlotte Burress²,
Alberto Striolo^{1,*}*

¹ Department of Chemical Engineering, University College London, WC1 E7JE London, UK

² Halliburton, Houston, Texas, USA

* Author to whom correspondence should be addressed: a.striolo@ucl.ac.uk

ABSTRACT

In gas clathrate hydrates, inclusion gas molecules stabilize crystalline water structures. In addition to being fundamentally interesting, gas hydrates attract significant practical attention because of their possible application in various high-tech technologies. However, gas hydrates pose health, safety, and environmental risks when they form within oil and gas pipelines, as well as within hydrocarbon-producing and treatment facilities. Among available strategies to control and sometimes prevent hydrate plugs formation is the use of surface-active low-molecular-weight compounds, known as anti-agglomerants (AAs). AAs prevent the agglomeration of small hydrate particles into large plugs. It is not clear whether AAs promote or frustrate hydrate growth. We present two molecular mechanisms by which AAs promote and frustrate, respectively, hydrate growth. Our results could lead to innovative methodologies for managing hydrates in high-tech applications, as well as for securing the safety of oil and gas operations.



Gas hydrates, inclusion compounds of water and gas molecules, form at low-temperature and high-pressure conditions. Gas hydrates offer an untapped and potentially significant resource of energy¹ and could help mitigate global warming through long-term CO₂ storage.² However, gas hydrates can block pipelines, causing production disruption and adverse environmental impact.³⁻⁵ To manage gas hydrates, chemicals known as hydrate inhibitors are often used. Thermodynamic inhibitors (TIs), such as methanol and ethylene glycol, shift the hydrate stability conditions to higher pressure and lower temperature. Although TIs are effective, high concentrations (up to 50 wt% of the water present in the systems) are necessary to prevent hydrate formation.^{6,7} In contrast, low dosage hydrate inhibitors (LDHIs) can be effective at concentrations as low as 0.5 wt%, but their mechanisms of action are not completely understood. Anti-agglomerants (AAs), usually surfactants expected to adsorb at water-oil and/or hydrate-oil interfaces,⁸ are a class of LDHIs. AAs inhibit the hydrate agglomeration process,⁹⁻¹² but it has been suggested,¹³⁻¹⁵ yet not confirmed, that AAs could potentially affect the hydrate-growth process. Among others, Karaaslan et al.¹⁵ reported experimental data according to which cationic surfactants promote or delay hydrate growth, depending on their concentration. The molecular mechanisms responsible for these observations are not understood.

To identify and quantify such molecular mechanisms, we report here classic molecular dynamics (MD) simulations used to monitor the growth of a hydrate seed in the presence of selected AAs at a fixed surface density of 0.44 molecules/nm². **Figure 1a** shows a schematic for the simulated system. We systematically changed the AA molecular features, focusing on AAs that yield different performance in preventing hydrate agglomeration in laboratory experiments.⁹ One of the AAs chosen for the present work (S₄) shows good performance, and one (S₈) shows poor performance. Experimental data are not available for the third AA (S₁). The three AAs have

one large hydrophilic head group and three hydrophobic tail groups. The difference in performance is apparently only due to the length of the short hydrophobic tail, highlighted in **Figure 1b**. The AAs that show good performance have a short tail of four carbon atoms, those with poor performance eight carbon atoms. During our simulations we monitor the growth of the hydrate seed (**Figure 1a**) by quantifying the evolution of the F4 order parameter, as calculated for the water molecules in the system.¹⁶ Additionally, we analyze the free-energy landscape as well as free-energy profiles experienced during hydrate growth by implementing the metadynamics framework¹⁷ and the umbrella sampling algorithm,¹⁸ respectively. We monitor several molecular-level properties during the simulations. Details regarding simulation models and algorithms are reported in Supporting Information (SI).

Our results, for the first time, demonstrate that AAs affect the hydrate growth process by means of their short alkyl tails and highlight the possible molecular mechanisms of action of these surface-active chemicals. Perhaps surprisingly, our simulations reveal that those AAs showing good performance in flow assurance can promote hydrate growth. They appear to do so by embedding their short alkyl tails within the growing hydrate crystal. The embedded tails stabilize the newly formed hydrate cages, which prevents adsorbed methane from escaping the hydrate structure. Our simulations also show that hydrate growth can be hindered by the AAs when the film of AAs formed at the water-hydrocarbon interface provides an effective barrier to methane diffusion from the hydrocarbon phase to the growing hydrate seed. The results obtained can have important implications in understanding the mechanism responsible for the performance of AAs in flow assurance. Additionally, the ability to promote hydrate growth could be exploited for promoting gas hydrate formation to boost high-tech applications, such as natural gas storage^{19–21} and seawater desalination,^{22,23} among others.^{24,25}

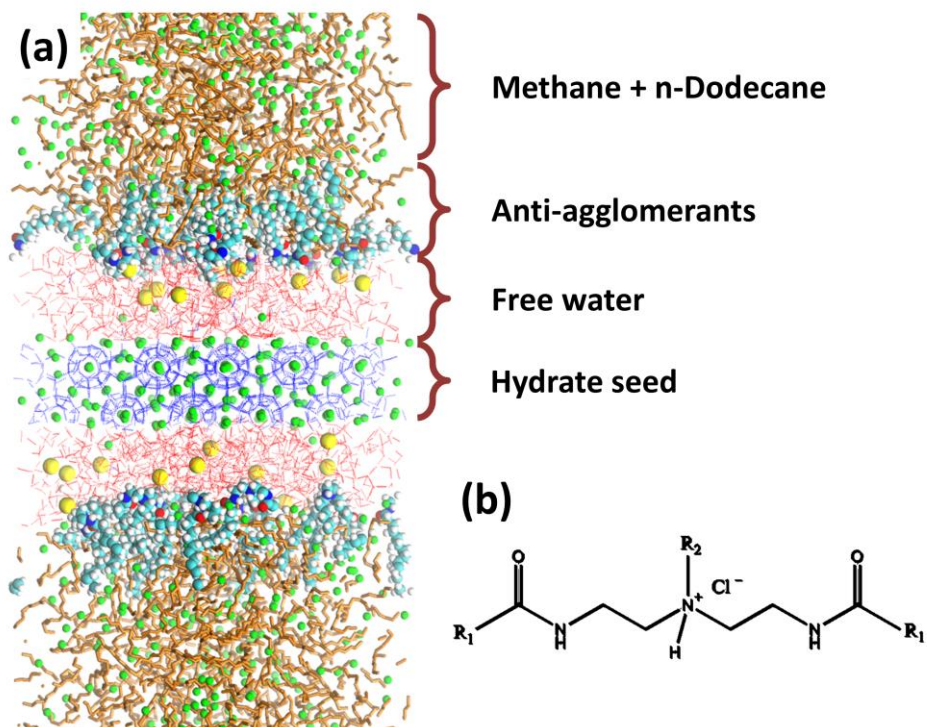


Figure 1. (a) Representative initial configuration. Green = methane, orange = n-dodecane, blue = water in hydrate seed, red = free water, yellow = chloride ions, and cyan and white spheres = AAs. (b) The molecular structure of the AAs considered in this work, which contain two long hydrophobic tails, R_1 , and one short hydrophobic tail, R_2 . The long R_1 tail is composed of one n-dodecyl chain in the systems considered here, and the short R_2 tail is composed of linear hydrocarbon chains of one, four, or eight carbon atoms. In our notation, one AA molecule is represented as S_N , where N indicates the number of carbon atoms in the short (S) tail.

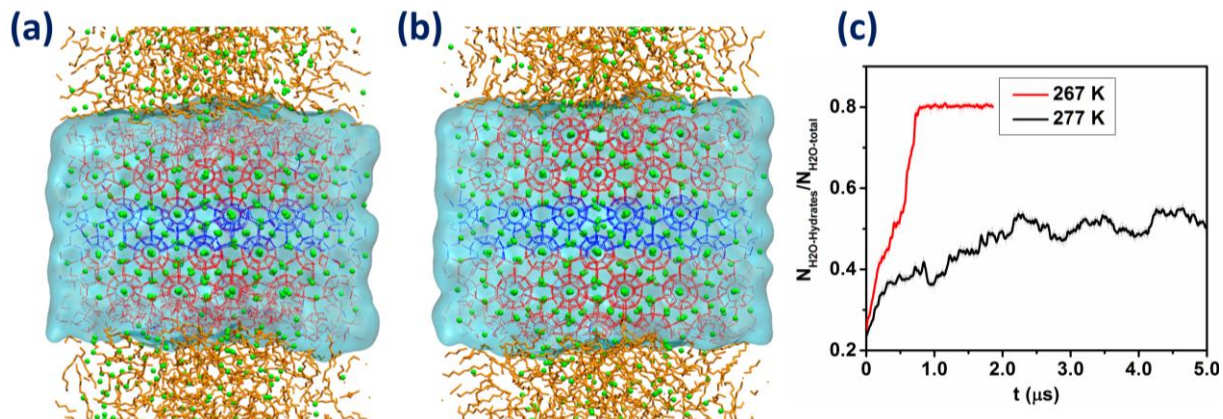


Figure 2. (a), (b) Simulation snapshots representing final configurations of the hydrate growth at 277 K and 267 K, respectively. Note that the thin water film between the hydrate and the hydrocarbon phase present at the beginning of the simulations (**Figure 1a**) has been converted into hydrate. (c) The growth of the hydrate as a function of time in terms of the ratio of water molecules in the hydrate substrate to the total number of water molecules present in the systems. Note that at the end of the growth process, some water molecules are disordered at the hydrate-hydrocarbon interfaces.

We first conducted simulations on systems without AAs. Simulation snapshots representing the final configurations of the hydrate grown at 277 K and 267 K (**Figure 2a** and **2b**, respectively), as well as quantitative results in terms of the evolution of the ratio of water molecules in the hydrate substrate over the total number of water molecules (**Figure 2c**), show that the hydrate seed grows faster and that the water-to-hydrate conversion reaches higher values at lower temperatures (almost 80% of the water available is converted to hydrate at 267 K vs. only 50% at 277 K). It is worth noting that the three-phase equilibrium conditions for methane hydrates using the TIP4P/Ice model for water are ~ 283 K at 10 MPa and ~ 293 K at 40 MPa, both of which underestimate the experimental melting temperatures by ~ 3 -4 K.²⁶ Therefore the three-phase equilibrium temperature corresponding to the pressure of 20 MPa in this study is expected to be between 283 K and 293 K. Thus the conditions chosen in this study are well within gas hydrate stability zone and correspond to sub-cooled systems. We refer to the SI (**Figure S1**) for details regarding the identification of water molecules in liquid or hydrate form. The higher growth rate at lower temperature is consistent with experimental observations, which show that such rate is proportional to subcooling.²⁷⁻²⁹ Our results show that some of the water molecules present in the simulated systems remain disordered at the hydrate-hydrocarbon interface at the end of the growth process. This is because of the presence of a “quasi-liquid” interfacial layer. According to Aman et al.,³⁰ the thickness of the quasi-liquid layer h depends on temperature as

$$h \propto \ln \left[\frac{1}{(T_0 - T)} \right] \quad (1)$$

In Eq. (1), T_0 and T are the hydrate melting temperature and the system temperature, respectively. From Eq. (1), it is expected that the lower the temperature, the thinner the quasi-liquid layer becomes, which is consistent with the results shown in **Figure 2c**.

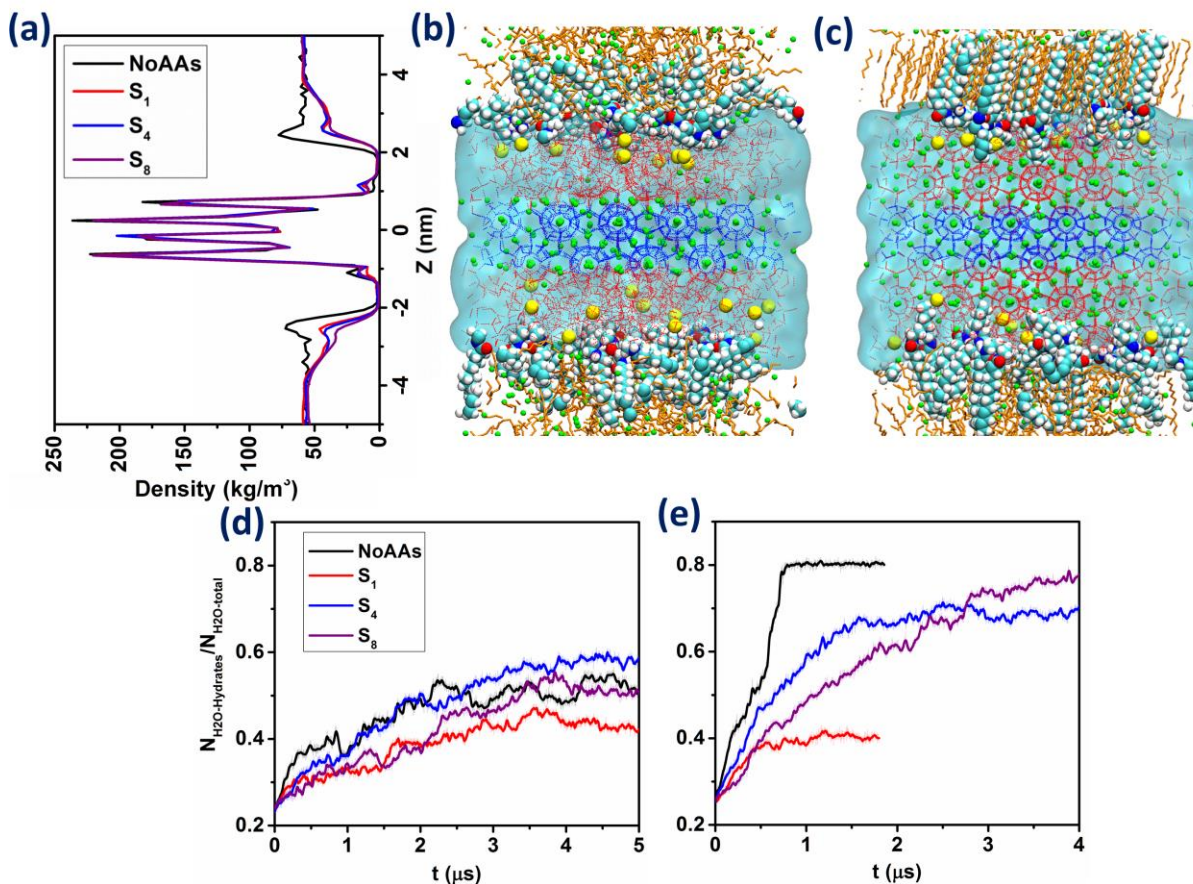


Figure 3. (a) Density profiles of methane along the Z direction of the simulation box in different systems at the beginning of the hydrate growth simulations; (b) and (c) simulation snapshots representing initial and final configurations, respectively, of the hydrate growth for the system with S₄ AAs at 267 K; (d) and (e) the evolution of the fraction of water molecules present in the system that belong to the growing hydrates as a function of time at 277 K and 267 K, respectively. Different curves in (d) and (e) represent results obtained using AAs with short tails of different lengths. **Figure 1b** shows the AA molecular structure details.

Simulations similar to those described in **Figure 2** were conducted for systems in the presence of AAs. **Figure 3** shows the results obtained. Compared to the system without AAs, at 277 K the presence of AAs lowers the hydrate growth rate in the early stage of the simulations ($t < 1 \mu\text{s}$) (**Figure 3d**). Our results suggest that these results are due to the fact that in the system without AAs, methane accumulates at the water-oil interfaces (**Figure 3a** and **Figure S2** of the SI). The availability of methane in relatively large concentrations near the growing hydrate seed provides a high driving force for growth.^{4,31} Our results suggest that the concentration of methane near the center of the water film near the growing hydrate does not depend on the AAs (**Figure S3** of the SI). As the observation time increases to $1 < t < 2.2 \mu\text{s}$, our results show that the growth rate plateaus. We observe that S_4 AAs promote faster hydrate growth compared to S_1 and S_8 AAs. The amount of water converted to hydrate at the end of the simulations increases in the order $S_4 \text{ AAs} > S_8 \text{ AAs} \sim \text{no AAs} > S_1 \text{ AAs}$. From these results, it appears that S_4 AAs promote hydrate growth, perhaps by stabilizing the hydrate structure. To clarify this possibility, we conducted additional simulations at 300 K. In these simulations, the methane hydrates obtained at the end of the growth simulations at 277 K are allowed to dissociate. Our results (**Figure S4**) indicate that the dissociation process is the slowest in the presence of S_4 AAs. We conclude that S_4 AAs can stabilize the hydrate structure, thus yielding higher growth rates and delaying hydrate melting compared to S_1 and S_8 .

Compared to the results obtained at 277 K, the growth rates at 267 K are higher for all systems (**Figure 3e**). For the most part, the trends discussed for 277 K holds for the 267 K simulations. The exception is the system with S_1 AAs, in which case the simulations show the formation of an ordered, highly packed AA film at the water-oil interface (**Figure S5** of the SI) at the early stages of the simulations (at $\sim 500 \text{ ns}$). The formation of these ordered AA layers is

temperature dependent.^{32–34} The molecular structure of this AA film is similar to that discussed previously.⁹ We expect these ordered interfacial AA films to delay the transport of methane from the hydrocarbon phase to the aqueous film near the growing hydrate, perhaps affecting hydrate growth as suggested by the results shown in **Figure 3**. Our results confirm that S₄ AAs promote faster hydrate growth compared to S₁ and S₈ AAs at the early stages of growth (less than ~1.5 μ s) even at 267 K. However, because of the formation of the ordered AA layer at the interface (**Figure 3c**), the final water conversion to hydrates in the presence of S₄ is lower compared to that obtained in the presence of S₈ AAs.

The results discussed so far suggest that S₄ AAs promote hydrate growth. Because the only difference among the three AAs considered here is the length of the short tails, it is possible that the n-butyl short tail interacts with the growing hydrate. Visual inspection of simulation snapshots, such as those shown in **Figure 3c**, reveals that indeed several n-butyl short tails penetrate the hydrate cages as the hydrates grow. Two fundamental questions stem from this qualitative observation: (1) why do the butyl tails penetrate the hydrate cages and (2) how are such molecular phenomena connected with the observed differences in hydrate growth rates.

To address the first question, well-tempered metadynamics simulations (WTM) were conducted. This protocol allows us to estimate the free-energy landscape sampled by the methyl group of one n-butyl short tail as it shifts from one location to another near or within the growing hydrate. Additionally, this approach allows us to identify the equilibrium state. The initial configuration for the WTM simulations was taken from the final configuration of the equilibration simulation at 277 K. One AA molecule whose n-butyl tail penetrates the hydrate was selected [**Figure 4** (top right)]. Those methane molecules of the n-butyl tail were then tagged. Two collective variables (CVs) were chosen: (1) the Z position of the methyl group and

(2) the number of tagged methane molecules that belong to the hydrate structure and are found within 1 nm of the methyl group and therefore coordinated with the n-butyl tail. CV1 allows us to monitor the position of the methyl group of the n-butyl tail with respect to the growing hydrate surface along the Z direction. CV2 allows us to monitor when the methyl group moves away from its position inside the hydrate cage (correspondingly, CV2 reduces from 10 to 0). **Figure 4** (bottom) shows the resultant free-energy landscape. Two free-energy basins are identified, corresponding to two favorable occupation positions for the methyl group. The first basin [CV1 \sim 7 nm and CV2 \sim 1] corresponds to a configuration in which the methyl group is in the oil phase [**Figure 4** (top left)]. The second free-energy basin [CV1 \sim 7.8 nm and CV2 \sim 10] corresponds to a configuration in which the methyl group has penetrated the hydrate structure [**Figure 4** (top right)]. The free-energy difference between the first and the second basins (\sim 3.4 \pm 1.4 kJ/mol) confirms that the n-butyl tails of S₄ AAs favorably integrate with the growing hydrate substrate. More details on the free energy differences are reported in SI (**Figure S6**).

With the aid of molecular distributions and molecular structure for both water and methane molecules surrounding the alkyl tails (**Figures S7** and **S8** of the SI), we concluded that the incorporation of the butyl tails of S₄ AAs into the hydrate does not perturb the hydrate structure. Instead, the n-butyl tails behave like guest methane molecules in the unperturbed hydrate. On the contrary, the methyl tails of S₁ AAs, which are short and connected directly to the bulky hydrophilic head group, perturb the hydrate structure (**Figure S7** and **S8** of the SI). S₈ AAs show moderate effects on the hydrate growth because the relatively long alkyl tails of S₈ AAs preferentially interact with the oil rather than the water molecules. Based on previous investigations,¹² and consistently with the proposed interpretation of experimental results, we suggest that when the short AAs tails penetrate and stabilize the growing hydrate crystal, the

AAs firmly attach to the hydrate surface, which should interfere with and prevent subsequent agglomeration processes.

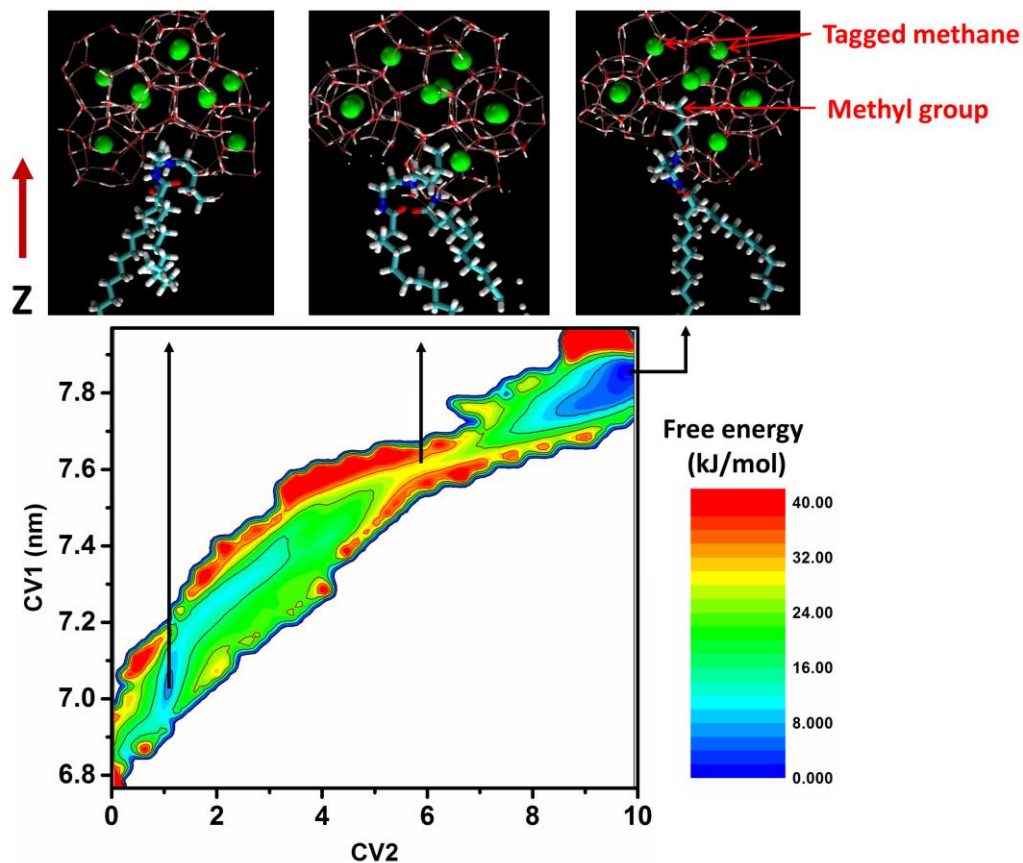


Figure 4. Bottom: two dimensional (2D) free-energy landscape as a function of the Z coordinate of the methyl group (CV1) and of the coordination number of methane molecules around the methyl group of S₄ AA short tails (CV2). Top: from left to right, configurations of the system correspondent to the first free-energy basin, the transition state, and the second free-energy basin, respectively. The activation energies for incorporation and release of the methyl group into/from the hydrate cage are ~ 43.3 kJ/mol ($18.8 k_B T$) and ~ 40.2 kJ/mol ($17.5 k_B T$), respectively.

To quantify how the interaction of the AAs tails with the hydrates relates to the observed growth rates, we implemented the umbrella sampling algorithm to calculate the PMF profiles experienced by one methane molecule moving from the growing hydrate surface to the bulk alkane phase. Details of the simulation protocol are reported in SI. The results of these calculations are shown in **Figure 5** and discussed further in SI. It is worth noting that the hydrate growth process is somewhat stochastic (**Figure 3d**) because of the competitive effects between the adsorption and desorption of methane at the hydrate growing interfaces. For example, once the methane molecules have approached the hydrate surface, they can diffuse back to the bulk water and perhaps to the alkane phase. The results in **Figure 5** show that the presence of the n-butyl tail next to the tagged methane molecule noticeably increases the depth of the free-energy basin ($\Delta E_0 \sim -7.1 \pm 1.6$ kJ/mol) near the growing hydrate surface, which is expected to favor hydrate growth. The energy barrier for desorption of methane from the hydrate surface, $\Delta E_0 + \Delta E_1$, highlighted in **Figure 5**, decreases from $\sim 19.4 \pm 0.6$ kJ/mol near the n-butyl tail, to $\sim 12.5 \pm 0.8$ kJ/mol in the absence of it. These results suggest that it is more difficult for methane molecules to desorb from the growing hydrate surface in the presence of the n-butyl tails. This could lead to faster growth rates in the presence of S₄ AAs.

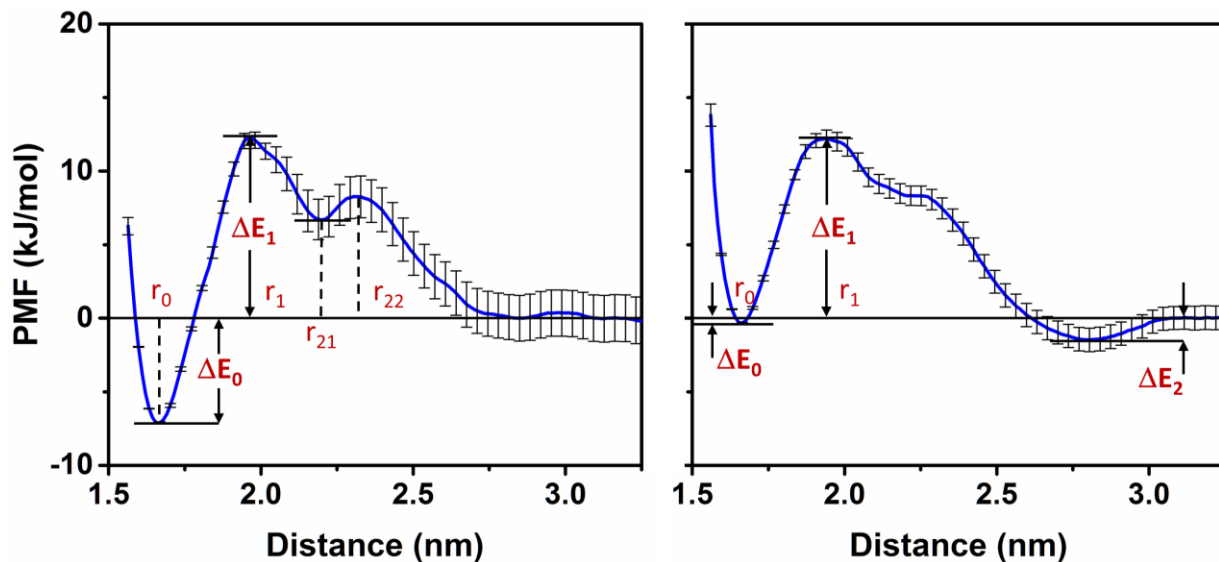


Figure 5. Potential of mean force (PMF) profiles obtained for the tagged methane molecule as it travels from the surface of the growing hydrate to the bulk alkane phase for a system with the tagged methane molecule next to a butyl tail penetrating the hydrate substrate (left) and for a system when the n-butyl tails next to the methane molecule are removed (right). Error bars are estimated from bootstrap analysis implemented in GROMACS.³⁵

In conclusion, we employed atomistic MD simulations to quantify the hydrate growth of methane hydrates in the presence of surfactants used as AAs. The AA molecules considered here contain amide and tertiary ammonium cation groups and have two n-dodecyl tails and one short alkyl tail. The length of the short tail strongly affects the performance of these AAs, according to experimental laboratory observations reported elsewhere.⁹ Our molecular simulations were analyzed in terms of evolution of the ratio of water in hydrate to total water, free-energy landscapes, the structure of water and methane around the short alkyl tails, and potential of mean forces. Surprisingly, we determined that the adsorption of AAs at the water-oil interface can affect the hydrate growth, according to two different mechanisms. As an inhibition effect, AAs

can reduce the concentration of methane at the interface, which lowers the driving force for hydrate growth. This effect is more pronounced when the interfacial AA layers become highly ordered and packed. As a growth enhancement effect, AAs with short n-butyl tails can stabilize cages near the growing hydrate. The results reported here are crucial for quantifying the hydrate growth mechanism in the presence of AAs, which could be exploited for designing new active compounds with hydrate-promoting or hydrate-inhibiting characters for different applications. However, hydrate growth in the presence of AAs is strongly dependent on temperature. The simulations conducted here were for sub-cooled systems. Should the temperature be increased, methane solubility in water decreases and the self-assembly of AAs at the water-hydrocarbon interface yields less-ordered structures. Should the temperature be decreased, molecular diffusion slows down, and it is possible that both hydrocarbons and surfactants undergo phase transitions. All these phenomena, and potentially others, affect the hydrate growth rate.

ASSOCIATED CONTENT

Supporting Information

Simulation details, data analysis methods, results for the evolution of the fraction of water molecules that belong to the hydrate structure during the hydrate dissociation process at 300 K, density profiles of methane, simulation snapshots, convergence of free-energy differences, distributions and structure of water and methane around the alkyl short tails of AAs, free-energy profiles, convergence analysis of the potential energy during hydrate growth process.

AUTHOR INFORMATION

Corresponding Author

*E-mail: a.striolo@ucl.ac.uk.

Notes

The authors declare no competing financial interest.

ACKNOWLEDGMENTS

The authors are grateful for the financial support provided by Halliburton and the UK Engineering and Physical Sciences Research Council (EPSRC) under grant number EP/N007123/1. Generous allocations of computing time were provided by the University College London Research Computing Platforms Support (LEGION) and by the National Energy Research Scientific Computing Center (NERSC) at Lawrence Berkeley National Laboratory. NERSC is supported by the Department of Energy (DOE) Office of Science under Contract No. DE-AC02-05CH11231.

ABBREVIATIONS

AAs, anti-agglomerants; RDFs, radial distribution functions; PMF, potential of mean force; SI, supporting information; WTM, well-tempered metadynamics.

REFERENCES

- (1) Walsh, M. R.; Hancock, S. H.; Wilson, S. J.; Patil, S. L.; Moridis, G. J.; Boswell, R.; Collett, T. S.; Koh, C. A.; Sloan, E. D. Preliminary Report on the Commercial Viability of Gas Production from Natural Gas Hydrates. *Energy Econ.* **2009**, *31*, 815–823.

- (2) Ersland, G.; Husebø, J.; Graue, A.; Kvamme, B. Transport and Storage of CO₂ in Natural Gas Hydrate Reservoirs. *Energy Procedia* **2009**, *1*, 3477–3484.
- (3) Dendy Sloan, E.; Koh, C. A.; Sum, A. *Natural Gas Hydrates in Flow Assurance*; Elsevier: Boston, 2011.
- (4) Dendy Sloan, E.; Koh, C. *Clathrate Hydrates of Natural Gases*, 3rd ed.; Crc Press-Taylor & Francis Group, 2007.
- (5) Malcolm A. Kelland. *Production Chemicals for the Oil and Gas Industry*; CRC Press, 2010; Vol. 72.
- (6) Storr, M. T.; Taylor, P. C.; Monfort, J. P.; Rodger, P. M. Kinetic Inhibitor of Hydrate Crystallization. *J. Am. Chem. Soc.* **2004**, *126*, 1569–1576.
- (7) Wu, R.; Aman, Z. M.; May, E. F.; Kozielski, K. A.; Hartley, P. G.; Maeda, N.; Sum, A. K. Effect of Kinetic Hydrate Inhibitor Polyvinylcaprolactam on Cyclopentane Hydrate Cohesion Forces and Growth. *Energy and Fuels* **2014**, *28*, 3632–3637.
- (8) Kelland, M. A.; Svartaas, T. M.; Øvsthus, J.; Tomita, T.; Mizuta, K. Studies on Some Alkylamide Surfactant Gas Hydrate Anti-Agglomerants. *Chem. Eng. Sci.* **2006**, *61*, 4290–4298.
- (9) Bui, T.; Phan, A.; Monteiro, D.; Lan, Q.; Ceglie, M.; Acosta, E.; Krishnamurthy, P.; Striolo, A. Evidence of Structure-Performance Relation for Surfactants Used as Antiagglomerants for Hydrate Management. *Langmuir* **2017**, *33*, 2263–2274.
- (10) Aman, Z. M.; Dieker, L. E.; Aspenes, G.; Sum, A. K.; Sloan, E. D.; Koh, C. A. Influence of Model Oil with Surfactants and Amphiphilic Polymers on Cyclopentane Hydrate

- Adhesion Forces. *Energy and Fuels* **2010**, *24*, 5441–5445.
- (11) Aman, Z. M.; Koh, C. A. Interfacial Phenomena in Gas Hydrate Systems. *Chem. Soc. Rev.* **2016**, *45*, 1678–1690.
- (12) Phan, A.; Bui, T.; Acosta, E.; Krishnamurthy, P.; Striolo, A. Molecular Mechanisms Responsible for Hydrate Anti-Agglomerant Performance. *Phys. Chem. Chem. Phys.* **2016**, *18*, 24859–24871.
- (13) Norland, A. K.; Kelland, M. The Crystal Growth Inhibition of Tetrahydrofuran Hydrate With Polyquaternary Ammonium Salts. *7th Int. Conf. Gas Hydrates (ICGH 2011)* **2011**, *69*, 483–491.
- (14) Kumar, A.; Bhattacharjee, G.; Kulkarni, B. D.; Kumar, R. Role of Surfactants in Promoting Gas Hydrate Formation. *Ind. Eng. Chem. Res.* **2015**, *54*, 12217–12232.
- (15) Karaaslan, U.; Parlaktuna, M. Surfactants as Hydrate Promoters? *Energy and Fuels* **2000**, *14*, 1103–1107.
- (16) Rodger, P. M.; Forester, T. R.; Smith, W. Simulations of the Methane Hydrate/methane Gas Interface near Hydrate Forming Conditions. *Fluid Phase Equilib.* **1996**, *116*, 326–332.
- (17) Barducci, A.; Bussi, G.; Parrinello, M. Well-Tempered Metadynamics: A Smoothly Converging and Tunable Free-Energy Method. *Phys. Rev. Lett.* **2008**, *100*.
- (18) Kästner, J. Umbrella Sampling. *Wiley Interdiscip. Rev. Comput. Mol. Sci.* **2011**, *1*, 932–942.

- (19) Gudmundsson, J. S. Method for Production of Gas Hydrates for Transportation and Storage. Google Patents July 16, 1996.
- (20) Katoh, Y.; Horiguchi, K.; Iwasaki, T.; Nagamori, S. Process for Producing Gas Hydrate Pellet. Google Patents August 16, 2011.
- (21) Koh, C. A.; Sloan, E. D.; Sum, A. K.; Wu, D. T. Fundamentals and Applications of Gas Hydrates. *Annu. Rev. Chem. Biomol. Eng.* **2011**, *2*, 237–257.
- (22) Park, K. nam; Hong, S. Y.; Lee, J. W.; Kang, K. C.; Lee, Y. C.; Ha, M. G.; Lee, J. D. A New Apparatus for Seawater Desalination by Gas Hydrate Process and Removal Characteristics of Dissolved Minerals (Na⁺, Mg²⁺, Ca²⁺, K⁺, B3⁺). *Desalination* **2011**, *274*, 91–96.
- (23) Babu, P.; Kumar, R.; Linga, P. Unusual Behavior of Propane as a Co-Guest during Hydrate Formation in Silica Sand: Potential Application to Seawater Desalination and Carbon Dioxide Capture. *Chem. Eng. Sci.* **2014**, *117*, 342–351.
- (24) Shi, X. J.; Zhang, P. Cold Storage by Tetra-N-Butyl Ammonium Bromide Clathrate Hydrate Slurry Generated with Different Storage Approaches at 40 Wt% Initial Aqueous Solution Concentration. *Int. J. Refrig.* **2014**, *42*, 77–89.
- (25) Eslamimanesh, A.; Mohammadi, A. H.; Richon, D.; Naidoo, P.; Ramjugernath, D. Application of Gas Hydrate Formation in Separation Processes: A Review of Experimental Studies. *J. Chem. Thermodyn.* **2012**, *46*, 62–71.
- (26) Michalis, V. K.; Costandy, J.; Tsimpanogiannis, I. N.; Stubos, A. K.; Economou, I. G. Prediction of the Phase Equilibria of Methane Hydrates Using the Direct Phase

- Coexistence Methodology. *J. Chem. Phys.* **2015**, *142*, 44501.
- (27) Uchida, T.; Ebinuma, T.; Kawabata, J.; Narita, H. Microscopic Observations of Formation Processes of Clathrate-Hydrate Films at an Interface between Water and Carbon Dioxide. *J. Cryst. Growth* **1999**, *204*, 348–356.
- (28) Freer, E. M.; Sami Selim, M.; Dendy Sloan, E. Methane Hydrate Film Growth Kinetics. *Fluid Phase Equilib.* **2001**, *185*, 65–75.
- (29) Taylor, C. J.; Miller, K. T.; Koh, C. A.; Sloan, E. D. Macroscopic Investigation of Hydrate Film Growth at the Hydrocarbon/water Interface. *Chem. Eng. Sci.* **2007**, *62*, 6524–6533.
- (30) Aman, Z. M.; Brown, E. P.; Sloan, E. D.; Sum, A. K.; Koh, C. A. Interfacial Mechanisms Governing Cyclopentane Clathrate Hydrate Adhesion/cohesion. *Phys. Chem. Chem. Phys.* **2011**, *13*, 19796.
- (31) Guo, G. J.; Rodger, P. M. Solubility of Aqueous Methane under Metastable Conditions: Implications for Gas Hydrate Nucleation. *J. Phys. Chem. B* **2013**, *117*, 6498–6504.
- (32) Tokiwa, Y.; Sakamoto, H.; Takiue, T.; Aratono, M.; Matsubara, H. Effect of Alkane Chain Length and Counterion on the Freezing Transition of Cationic Surfactant Adsorbed Film at Alkane Mixture – Water Interfaces. *J. Phys. Chem. B* **2015**, *119*, 6235–6241.
- (33) Sloutskin, E.; Bain, C. D.; Ocko, B. M.; Deutsch, M. Surface Freezing of Chain Molecules at the Liquid–liquid and Liquid–air Interfaces. *Faraday Discuss.* **2005**, *129*, 339–352.
- (34) Tamam, L.; Pontoni, D.; Sapir, Z.; Yefet, S.; Sloutskin, E.; Ocko, B. M.; Reichert, H.; Deutsch, M. Modification of Deeply Buried Hydrophobic Interfaces by Ionic Surfactants. *Proc. Natl. Acad. Sci.* **2011**, *108*, 5522–5525.

- (35) Hub, J. S.; De Groot, B. L.; Van Der Spoel, D. G-Whams-a Free Weighted Histogram Analysis Implementation Including Robust Error and Autocorrelation Estimates. *J. Chem. Theory Comput.* **2010**, *6*, 3713–3720.